ACS SENSORS

pubs.acs.org/acssensors

Article

Detection of SARS-CoV-2 Virus Amplification Using a Crumpled Graphene Field-Effect Transistor Biosensor

Insu Park,[○] Jongwon Lim,[○] Seungyong You, Michael Taeyoung Hwang, Jaehong Kwon, Katherine Koprowski, Sungdae Kim, John Heredia, Sarah A. Stewart de Ramirez, Enrique Valera,* and Rashid Bashir*

Cite This: https://doi.org/10.1021/acssensors.1c01937

Read Online

ACCESS | Metrics & More | Article Recommendations | Supporting Information

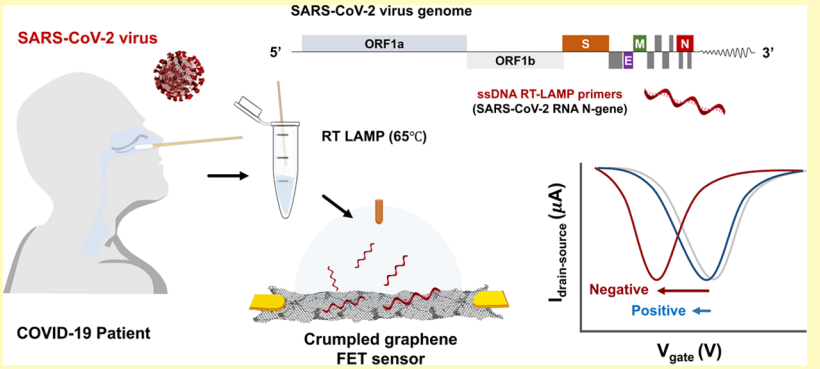

ABSTRACT: The rapid and unexpected spread of SARS-CoV-2 worldwide has caused unprecedented disruption to daily life and has brought forward critical challenges for public health. The disease was the largest cause of death in the United States in early 2021. Likewise, the COVID-19 pandemic has highlighted the need for rapid and accurate diagnoses at scales larger than ever before. To improve the availability of current gold standard diagnostic testing methods, the development of point-of-care devices that can maintain gold standard sensitivity while reducing the cost and providing portability is much needed. In this work, we combine the amplification capabilities of reverse transcriptase loop-mediated isothermal amplification (RT-LAMP) techniques with high-sensitivity end-point detection of crumpled graphene field-effect transistors (cgFETs) to develop a portable detection cell. This electrical detection method takes advantage of the ability of graphene to adsorb single-stranded DNA due to noncovalent $\pi-\pi$ bonds but not double-stranded DNA. These devices have demonstrated the ability to detect the presence of the SARS-CoV-2 virus in a range from 10 to 10^4 copies/μL in 20 viral transport medium (VTM) clinical samples. As a result, we achieved 100% PPV, NPV, sensitivity, and specificity with 10 positive and 10 negative VTM clinical samples. Further, the cgFET devices can differentiate between positive and negative VTM clinical samples in 35 min based on the Dirac point shift. Likewise, the improved sensing capabilities of the crumpled gFET were compared with those of the traditional flat gFET devices.

KEYWORDS: *crumpled graphene FET biosensor, flat graphene FET biosensor, SARS-CoV-2, RT-LAMP, COVID-19, VTM clinical samples*

As it is well known, reverse transcription-polymerase chain reaction (RT-PCR) is the current gold standard diagnostic method for the COVID-19 disease.[1] This molecular detection technology, which detects the genetic material of the SARS-CoV-2 virus, has high accuracy when performed by a healthcare professional.[2] However, some inherent PCR analysis features, such as the need for temperature cycling and laboratory-based protocols for viral isolation, lysis, and removal of inhibiting materials, make this technique difficult to adapt for miniaturization, portability, and point-of-care detection.[3,4] Isothermal approaches eliminate the need for precise thermal cycles to achieve RNA amplification and provide additional advantages such as the possible elimination of the viral purification step and the simplification of the instrumentation complexity.[1] It is due to these advantages and the aforementioned inconveniences of RT-PCR that isothermal amplification-based approaches have recently attracted significant attention for the detection of SARS-CoV-2 at the point-of-care.[1]

Received: September 9, 2021
Accepted: November 30, 2021

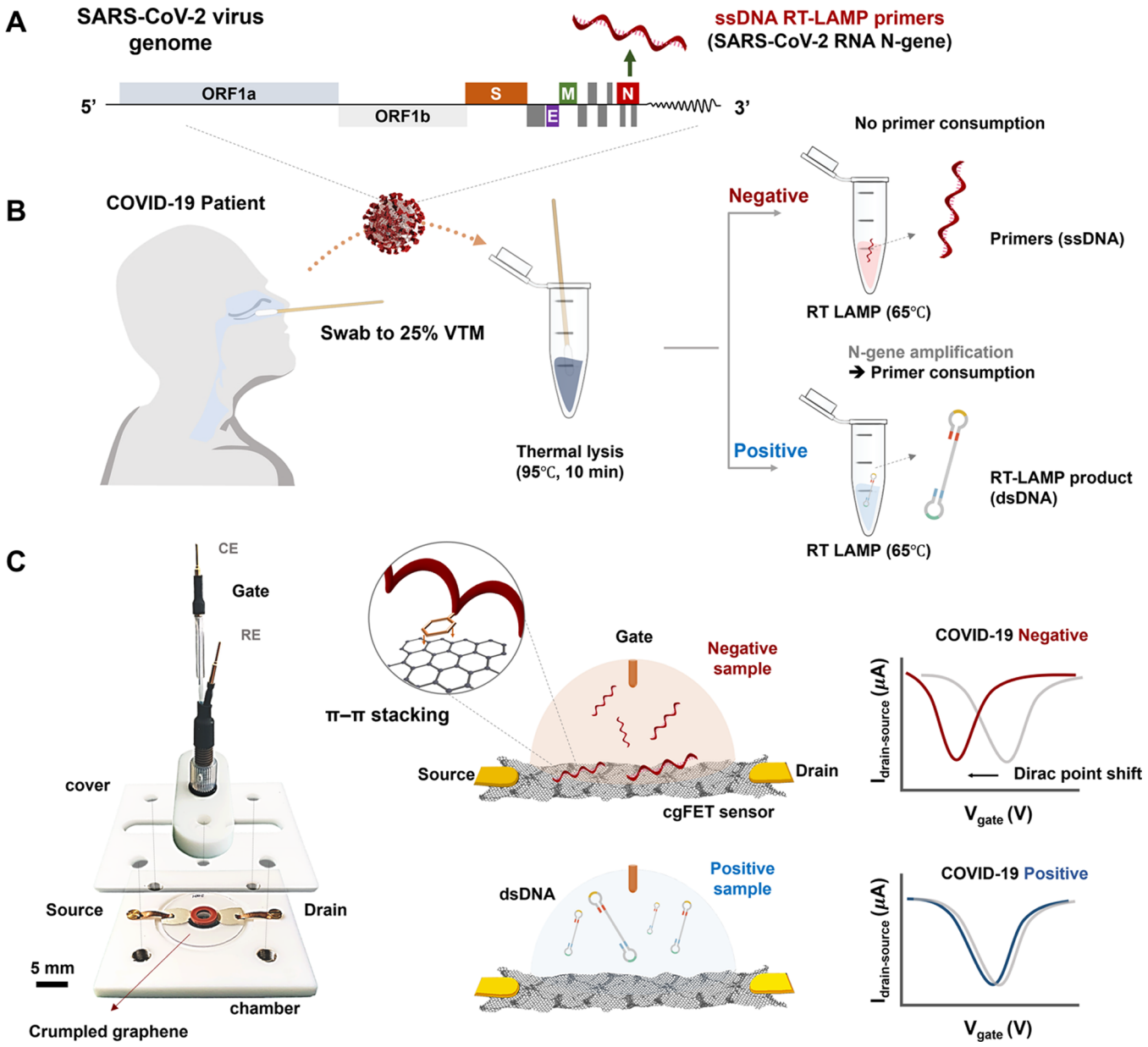

Figure 1. Schematic diagram of crumpled graphene field-effect transistor-based (cgFET) SARS-CoV-2 virus detection in VTM clinical samples. (A) Genome map shows the target site on the SARS-CoV-2 N-gene. Five RT-LAMP primers (F3, B3, FIP, BIP, LB) specific to the N-gene were used. (B) Workflow of the isothermal amplification prior to cgFET sensing. Detection is based on the consumption of RT-LAMP primers during the amplification reaction. RT-LAMP was used to amplify SARS-CoV-2 RNA within the N-gene region from VTM clinical samples resulting in primer consumption. (C) Crumpled graphene is used as a sensing material for the ionic gate-based FET, and the chamber is fabricated for isolating virus samples. CE: counter electrode, RE: reference electrode. Dimensions of crumpled graphene and chamber system can be seen in the Supporting Information (Figures S2 and S3). N-gene primers are attached to the crumpled graphene surface by $\pi-\pi$ stacking. Primer adsorption on the graphene surface shows a large Dirac point shift in negative samples.

Yet, the availability of the COVID-19 vaccine has not diminished the importance of the need for diagnosis. As of August 15, 2021, less than 60% of the population ≥12 years of age has been fully vaccinated in the U.S.[5] Moreover, even after vaccination, diagnostics remain important because vaccinated people may still carry and transmit the live virus and the duration for which immunity lasts after infection or vaccination is not yet known.[1,6,7]

Since the current pandemic brought the point-of-care (POC) diagnostic tests into the spotlight, many POC devices for the diagnosis of COVID-19 have been reported in the literature or have been awarded an Emergency Use Authorization (EUA) over the past year. Although most of them rely on visual readout techniques,[3,8−10] several electrical readout options are also available. Electrical readout options reduce cost by avoiding the necessity of fluorophores, lasers, LEDs, cameras, etc. Among the electrical readout options, special attention is paid to graphene-based biosensors.[11] Likewise, isothermal amplification-based approaches, such as RT-LAMP, have recently generated significant interest for the detection of the SARS-CoV-2 virus due to the simplicity of this technology and the ease of translation into a point-of-care device.[1]

Graphene, a two-dimensional material, is attracting significant attention for the development of sensing platforms due to

https://doi.org/10.1021/acssensors.1c01937
ACS Sens. XXXX, XXX, XXX−XXX

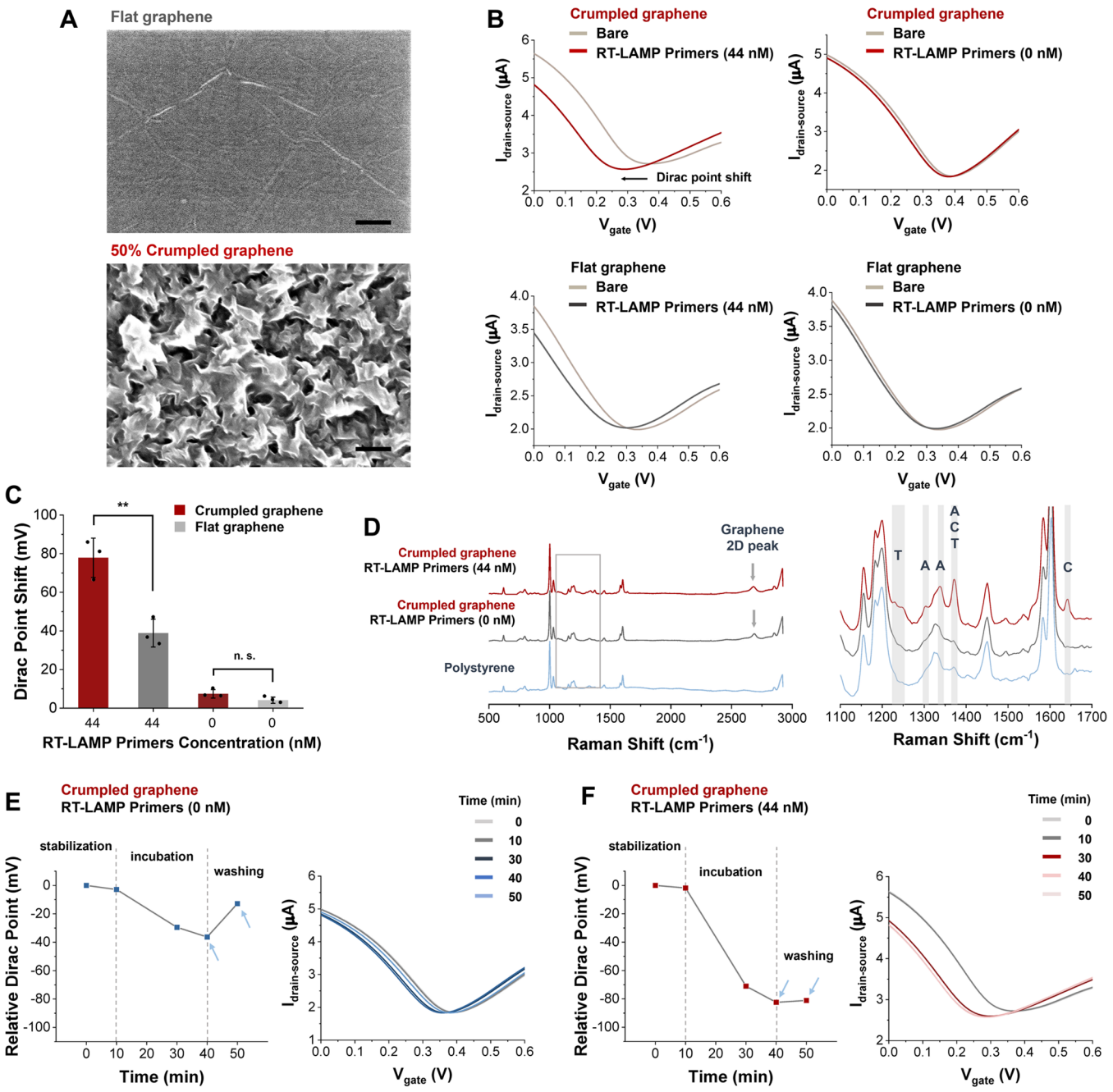

Figure 2. Direct detection of SARS-CoV-2 N-gene primers on flat and crumpled graphene FET. (A) SEM images of the flat and crumpled graphene surface, scale bar is 100 nm. (B) Examples of $I-V$ curves of flat and crumpled graphene FET sensors for primer adsorption. (C) Bar plot summarizing the Dirac point shifts obtained after primer adsorption on flat and crumpled graphene FETs ($n = 3$). n.s.: not significant, $^{*}P < 0.05$, $^{**}P < 0.005$. (D) Raman spectra of the polystyrene substrate and crumpled graphene surface after testing RT-LAMP primers (left). The close-up characterization of the spectra within the rectangular area (right) demonstrates the specific adenine, cytosine, and thymine Raman peaks for the primer-adsorbed crumpled graphene. (E, F) End-point measurement of the Dirac point shift at various reaction times in the absence (E) or presence (F) of primers. A negligible voltage change is obtained during the stabilization step, while the presence of primers produces a significant variation in the Dirac point. The total shift is calculated after the washing steps. Light blue arrows represent the washing step. The stability of primer adsorption on cgFET during measurement is shown in Figure S5.

its extraordinary properties, including ambipolar field effect, high electrical conductivity, high carrier mobility, large specific area, biocompatibility, mechanical strength, and flexibility.[11,12] In particular, the combination of graphene and field-effect transistors has produced a new generation of biosensing devices, gFET biosensors, with potential application in clinical diagnosis, point-of-care testing, and on-site detection, all the while offering high-sensitivity, low-cost, and high-throughput detection.[13−15] Although gFET biosensors generally use flat graphene as the sensing area, innovation in this field has recently been reported with the use of crumpled graphene.[12,16] Crumpled graphene, a structure that can be fabricated on different thermally[12] or mechanically[17] flexible and stretchable substrates, is a 3D engineered material. When crumpled graphene is combined with FET transistors (crumpled gFET, cgFET), ultra-high-sensitivity nucleic acid detection (zM

https://doi.org/10.1021/acssensors.1c01937
ACS Sens. XXXX, XXX, XXX−XXX

range) can be accomplished.[12,16] It is known that the Debye length in the ionic solution increases in the convex region of the crumpled graphene.[12] Therefore, more DNA is present inside the Debye length, which makes crumpled graphene more electrically susceptible to the negative charge of DNA.[12] This can be translated into a larger Dirac point shift.

In this study, we present a crumpled graphene FET (cgFET) biosensor to detect the presence of the SARS-CoV-2 virus in viral transport media (VTM) samples from patients. The developed point-of-care device was validated by the analysis of 20 VTM clinical samples (10 known positive and 10 known negative samples) with perfect sensitivity and specificity. This biosensor uses a conventional isothermal RT-LAMP amplification method,[3,18] and sensing is based on the detection of the consumption of primers after the amplification reaction. Our electrical device has shown the ability to detect the spiked SARS-CoV-2 virus in the range from 10 to 10^4 copies/μL and differentiate positive from negative clinical patient samples after 35 min of amplification. Using the fact that the primers are consumed during the amplification, we took advantage of graphene's ability to discriminate between double-stranded DNA (dsDNA) and single-stranded DNA (ssDNA). Thus, the ssDNA RT-LAMP primers against N-gene that were not consumed during the amplification event were strongly adsorbed on the cgFET surface through noncovalent $\pi-\pi$ stacking interactions. This adsorption of ssDNA produced a shift in the Dirac voltage that was correlated to the presence of the virus. Thus, shifts above the detection threshold indicate negative samples, while shifts below the detection threshold indicate positive samples. In this work, we fully characterized our cgFET device and compared its performance with a flat graphene FET (fgFET) biosensor. We also characterized the adsorption of primers on both flat and crumpled graphene surfaces after measuring the Dirac point shifts, which was verified by both Raman spectroscopy and atomic force microscopy techniques.

Although our group has recently demonstrated the improved sensitivity of crumpled graphene[12,19] and indirect detection based on primer consumption,[16] here, we further demonstrate the effectiveness of this technology through the detection of SARS-CoV-2 virus amplification and end-point measurement of the Dirac point shift at various reaction times. The SARS-CoV-2 virus was detected from VTM clinical samples in a portable detection cell. Moreover, herein, pretreatment of the clinical samples entailed simple dilution and short (10 min) thermal lysis, which eliminated the need for RNA purification kits. Although other contributions have reported the use of the graphene-based FET for the detection of the SARS-CoV-2 virus,[11,20] this is the first time, to the best of our knowledge, that crumpled graphene FET biosensors are used for this application. We also optimized the RT-LAMP reaction time using multiple end-point experiments and the corresponding statistical comparison analysis, resulting in shortened reaction time (from 1 h to 30 min). In addition, our device has achieved detection based on primer consumption, which is an improvement over other detection techniques that use the conjugation of expensive capture molecules on the graphene surface. Furthermore, this biosensor utilized the inherently high sensitivity of crumpled graphene and the amplification assays.

RESULTS AND DISCUSSION

Point-of-Care Crumpled Graphene FET Biosensor for SARS-CoV-2 Virus Detection. The process flow for the detection of SARS-CoV-2, based on the use of the developed crumpled graphene field-effect transistor (cgFET) is shown in Figure 1. Single-stranded DNA (ssDNA) RT-LAMP primers, specifically targeting the N-gene region, were selected for the isothermal RT-LAMP amplification reaction (Figure 1A). In the detection protocol (Figure 1B), the sample collected from the patient using a nasopharyngeal (NP) swab, was first transferred to the VTM solution. The sample was diluted 1:1 in Tris EDTA (TE) buffer and then thermal lysis (95 °C, 10 min, heating block) was performed to efficiently disrupt the viruses to release the RNA for amplification, while also inactivating the nucleases that are present in unpurified samples. The lysed sample was mixed again with TE buffer (1:1) and added to the RT-LAMP reaction mix, and the amplification reaction was conducted (65 °C, 50 min). With regards to the SARS-CoV-2 negative sample, the ssDNA RT-LAMP primers against N-gene are not consumed during the amplification event due to the absence of the RNA target. On the other hand, in the event of a positive sample, the primers will form dsDNA molecules during the amplification reaction. After the amplification reaction is completed, the amplified sample is transferred to the cgFET detection cell to perform the electrical measurement (Figure 1C). During sample incubation, the ssDNA molecules available were strongly adsorbed on the cgFET surface through noncovalent $\pi-\pi$ stacking interactions, which included noncovalent interactions between the aromatic rings of the graphene and exposed bases of the oligonucleotides. Thus, the shift in the Dirac point voltage is correlated to the presence or absence of the virus. Negative samples result in a large Dirac point shift due to the availability of ssDNA molecules. Meanwhile, a small Dirac point shift is expected for positive samples as most of the primers were consumed during the amplification event. The fabricated cgFET detection cell provided insulation for the sample and prevented sample evaporation during the incubation step.

Detection of ssDNA Primer Molecules Using the Crumpled Graphene FET Biosensor. The ability of the cgFET device to detect the presence of ssDNA molecules was assessed by calculating the Dirac point shifts produced when the RT-LAMP primers are added to the device. The concentration of primers added was the same as that required for the amplification assay. In Figure 2A, the morphology of 50% crumpled graphene was compared to the morphology of flat graphene by scanning electron microscopy (SEM). The random and large wrinkles created in the crumpled graphene structure are known to increase the Debye length,[12] resulting in enhanced changes in electrical conductance when the DNA strand is attached to the surface. In our previous study, the electrostatic and charge distributions of DNA and ions near flat and deformed graphene surfaces were studied using molecular dynamics (MD) simulations to investigate the effect of ionic screening of DNA molecules.[12,19] The deep and narrow trench on deformed graphene can provide low ionic screening for an absorbed DNA molecule with increasing EDL length. As a result, deformed graphene can reduce the counter-ion screening of the DNA molecules, which can enhance the detection sensitivity of cgFET. In addition, density functional theory (DFT) and GW methods were used to calculate the

https://doi.org/10.1021/acssensors.1c01937
ACS Sens. XXXX, XXX, XXX−XXX

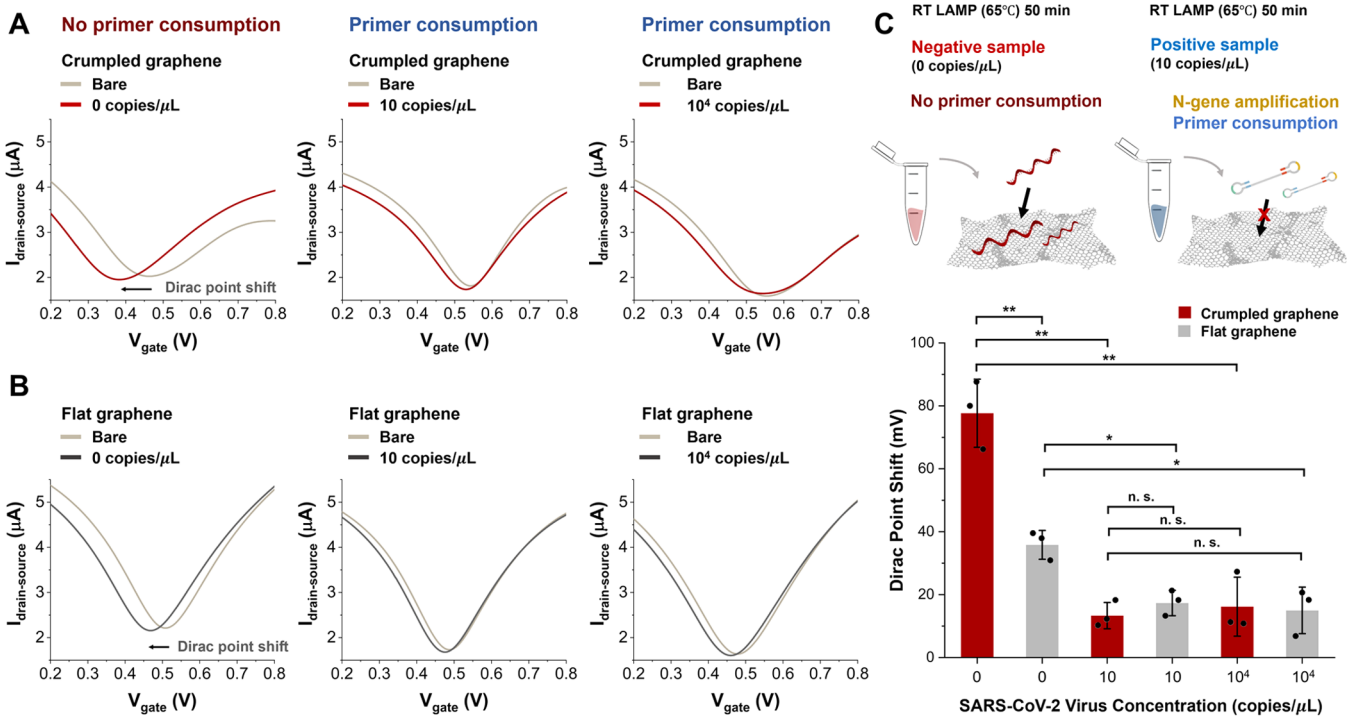

Figure 3. Detection of the inactivated SARS-CoV-2 virus spiked in 25% VTM on flat and crumpled graphene FET biosensors. Representative example of $I-V$ curves of (A) crumpled and (B) flat graphene FET sensors for primer absorption from amplified (10 and 10^4 copies/μL) and unamplified (0 copies/μL) virus spiked in VTM. (C) Top panel: schematic of the primers consumption approach. Bottom panel: bar plot summarizing the Dirac point shifts obtained after amplification of the inactivated SARS-CoV-2 virus on flat and crumpled graphene FETs (n = 3). n.s.: not significant, *P < 0.05, **P < 0.005.

bandgap for flat and crumpled graphene in the absence and presence of DNA bases.[12] Bandgap opening on deformed and crumpled graphene by adding DNA allows an exponential change in the source−drain current from small numbers of charges. Therefore, the deformation of graphene can enhance the detection sensitivity by reducing charge screening coupled with the opening of the bandgap, which can induce more changes in graphene carrier charge density from DNA absorption leading to a larger Dirac point shift. This enhancement in the sensitivity can be seen in Figure 2B,C where the changes in the source−drain current and Dirac point shifts of the cgFET were compared with the changes produced when using a fgFET biosensor. These figures show a statistically significant variation in the Dirac point for the same concentration of primers when using the cgFET in comparison to the fgFET. Dirac point changes were measured on the fgFET and cgFET biosensors in the presence (44 nM) or absence (0 nM) of RT-LAMP primers. Adsorption of negatively charged single-stranded DNA triggered a left shift of the Dirac point, which describes the n-doping of the primers on graphene.[21] Likewise, the correlation of the changes in the Dirac point with the concentration of added primers demonstrates that the variation in the Dirac point could be used as a figure of merit to detect the presence of primers. Also, the smaller variations were observed using the fgFET device and the differences in the signal-to-noise ratio (SNR) demonstrate better sensitivity of the developed cgFET sensor (Figure 2C). Finally, the adsorption of primers on the graphene surface was verified by means of Raman spectroscopy (Figure 2D). This technique was used to detect the predominant Raman spectra of ssDNA in crumpled graphene after measuring the $I-V$ curves. The predominant Raman peak of adenine at 1304, 1336, and 1372 nm, cytosine at 3172, 1643 nm, and thymine at 1230 and 1372 nm,[22] were observed in crumpled graphene tested with 44 nM RT-LAMP primers, whereas the peak was not observed in crumpled graphene tested without primers (Figure S1).

In addition to the end-point detection, the ability of end-point measurement of Dirac point in various reactions was also demonstrated. Figure 2E,F shows the variation of the Dirac point when using the crumpled graphene FET device. End-point measurement analysis shows, first, the negligible voltage changes during the stabilization step, and then the primer concentration-dependent variation of the Dirac point. The total shift is calculated after the washing steps.

Detection of the Inactivated SARS-CoV-2 Virus Spiked in VTM Solution. The ability of the cgFET device to detect the presence of the SARS-CoV-2 virus was assessed by spiking known concentrations of inactivated virus spiked in VTM solution, using these samples to conduct RT-LAMP assays, incubating the amplified product on the device, and calculating the Dirac point shifts produced after incubation.

As an off-chip control, the RT-LAMP amplification reaction was tested not only electrically (using the cgFET devices), but also optically (using a commercial thermocycler).

To do this, EvaGreen, a green fluorescence intercalating dye that can fit between base pairs of DNA molecules, was included in the reaction. The inactivated SARS-CoV-2 virus, ranging from 0 to 10^4 copies/μL, were spiked in 25% VTM solutions, and the RT-LAMP reaction was conducted at 65 °C (50 min). The amplification curves obtained from the thermocycler (reaction control) can be found in Figure 5A. The amplification threshold time was calculated at 20% of the normalized fluorescence signal. These results demonstrated

https://doi.org/10.1021/acssensors.1c01937
ACS Sens. XXXX, XXX, XXX−XXX

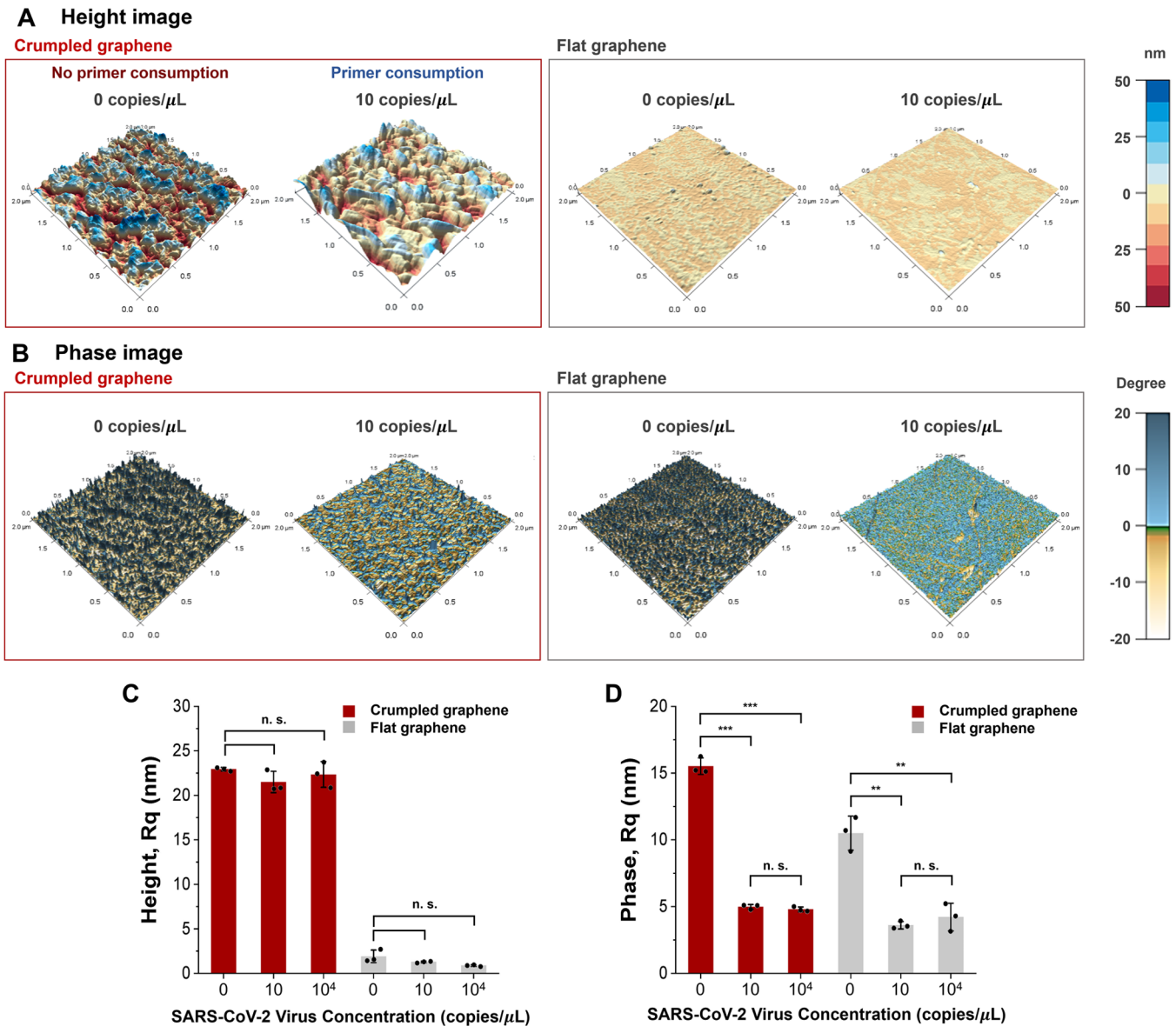

Figure 4. AFM images of flat and crumpled graphene surfaces showing primer adsorption after amplification of the inactivated SARS-CoV-2 virus spiked in 25% VTM. (A) Height images and (B) phase images of the flat and crumpled graphene surface after the cgFET test of 10^4 and 0 copies/μL virus samples. (C) Corresponding quantification of surface roughness (Rq) analyzed either from height images (C) or phage images (D) of flat and crumpled graphene surfaces tested with amplified and unamplified spiked SARS-CoV-2 samples. All of the data points were obtained for three cycles from different devices. n.s.: not significant, *P < 0.05, **P < 0.005, ***P < 0.0005.

that this reaction could detect at least 10 copies/μL of viral RNA.

After successful amplification was confirmed by the thermocycler amplification curves, the amplified products of the tested virus concentrations (0, 10, and 10^4 copies/μL) were diluted 100-fold in 0.1× phosphate-buffered saline (PBS). The diluted samples were transferred to both the cgFET and fgFET devices, and the variations in the Dirac point were measured (before and after adding the amplified product). The raw $I-V$ curves and the corresponding Dirac point shifts in the cgFET and fgFET devices can be seen in Figure 3A,B, respectively. In the case of blank samples (0 copies/μL of virus in the sample), a large Dirac point shift was obtained since primers were not consumed during the amplification reaction. However, as can be seen in Figure 3C, a larger Dirac point shift was found for the crumpled graphene sensor (~77.64 mV) compared to the shift obtained with the flat graphene sensor (~35.83 mV). On the other hand, when the virus was present in the sample (primers were consumed during the amplification reaction), the Dirac point shift obtained was smaller (<30 mV for both devices). The significance level of statistical difference between positive and negative samples was increased (the p-value was decreased from <0.05 to <0.005, Figure 3C) and therefore the signal-to-noise ratio and detection sensitivity were improved. It is important to achieve such high SNR since the amplified samples include several components that can bind nonspecifically to the graphene surface, thereby leading to the overlap of the Dirac point shift between two sample groups. Finally, the adsorption of the primers was also verified in both flat and crumpled graphene devices through atomic force microscopy (AFM) characterization of height and phase images (Figure 4). As can be seen

https://doi.org/10.1021/acssensors.1c01937
ACS Sens. XXXX, XXX, XXX−XXX

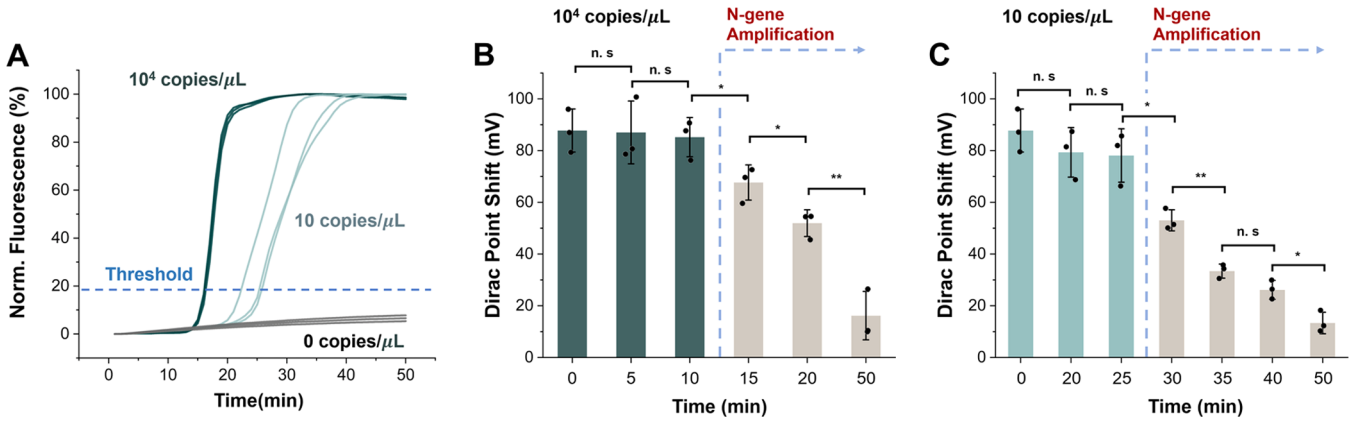

Figure 5. Detection of the inactivated SARS-CoV-2 virus spiked in 25% VTM samples using the cgFET biosensor. (A) Off-chip control. Normalized fluorescence data (n = 3) of 10^4, 10, and 0 copies/μL virus samples. RT-LAMP amplification threshold is determined at 20% of the normalized fluorescence signal. (B) Bar plot summarizing the Dirac point shifts of cgFETs obtained after amplification of 10^4 copies/μL virus samples with 0, 5, 10, 15, 20, and 50 min of RT-LAMP amplification time (n = 3). (C) Bar plot summarizing the Dirac point shifts obtained after amplification of 10 copies/μL virus samples with 0, 20, 25, 30, 35, 40, and 50 min of RT-LAMP amplification time on cgFETs (n = 3). n.s.: not significant, *P < 0.05, **P < 0.005.

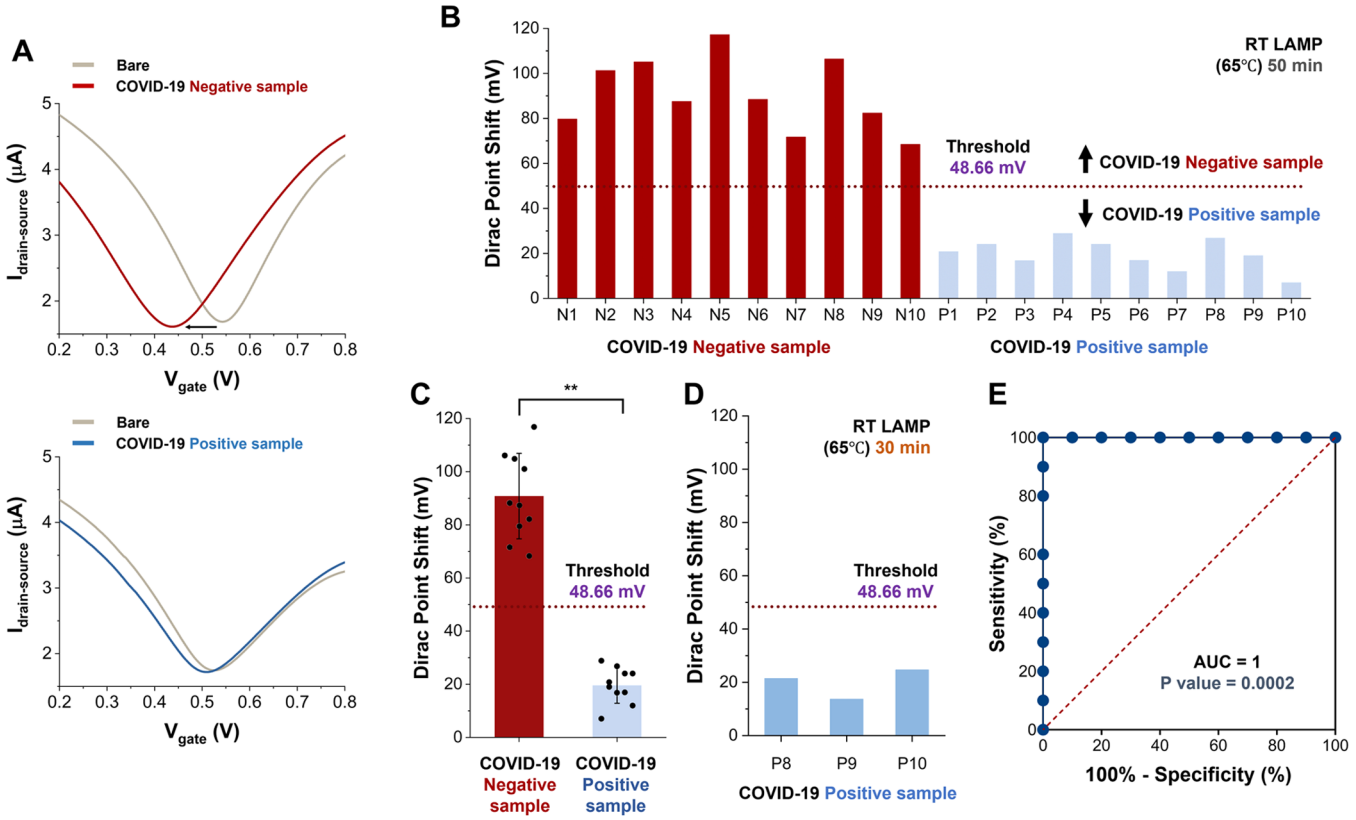

F

Sample	Reaction format	# true positives	# false positives	# true negatives	# false negatives	PPV (%)	NPV (%)	Sensitivity (%)	Specificity (%)
VTM clinical samples	RT-LAMP	10	0	10	0	100	100	100	100

Figure 6. Detection of the SARS-CoV-2 virus in 25% VTM clinical samples. (A) Representative example of I–V curves of crumpled graphene FET sensors for primer adsorption from SARS-CoV-2 positive and negative clinical samples in 25% VTM after isothermal amplification. (B) Bar plot of the Dirac point shift of 10 known positive and 10 known negative clinical samples (RT-LAMP; 65 °C, 50 min) on cgFET. The decision threshold (48.66 mV, 95% CI = 72.25−100%) was determined using ROC analysis. (C) Bar plot summarizing the average Dirac point shift of positive and negative clinical SARS-CoV-2 samples (RT-LAMP; 65 °C, 50 min) on the crumpled graphene FET. **P <0.005. (D) Bar plot of the Dirac point shift of 3 known positive clinical samples with the lowest viral load (RT-LAMP; 65 °C, 30 min) on the cgFET. (E) ROC curve analysis for positive and negative SARS-CoV-2 clinical samples in 25% VTM. (F) Summary of the performance of the cgFET biosensor for SARS-CoV-2 VTM clinical samples.

https://doi.org/10.1021/acssensors.1c01937
ACS Sens. XXXX, XXX, XXX−XXX

in Figure 4A,C, AFM height images do not distinguish between the presence or absence of primers. This is because the height of the ssDNA is ∼1 nm, which is negligible by AFM when DNA is adsorbed with a $\pi-\pi$ stacking structure on both flat and crumpled graphene surfaces. Likewise, the signal in the height images is higher in the crumpled graphene device than in flat graphene due to the morphology of the crumpled surface. On the other hand, as can be seen in Figure 4B,D, the AFM phase images confirmed the presence of primers for the negative samples. The phase shift between the cantilever oscillation and the driving signal enables chemical surface mapping that relies on inelastic interaction between the tip and surface, such as stiffness/smoothness and adhesion.[23] A clear difference in the signal was obtained in the phase images when comparing the positive with the negative samples for both devices. However, the difference was more significant for the cgFET than for the fgFET, which indicated that more primers were adsorbed on crumpled graphene than on flat graphene. Together, these results demonstrate the enhanced ability of the cgFET device to distinguish positive from negative samples. Cross-section plots of AFM height and phase images can be seen in the Supporting Information (Figure S2).

Analysis of the Required Amplification Time to Distinguish Positive Samples from Negative Sample. In the previous section, we demonstrated that SARS-CoV-2 positive samples (in the range from 10 to 10^4 copies/μL) can be distinguished from negative samples using graphene devices after 50 min of amplification. However, to show that shorter amplification times could also be used, multiple end-point experiments, in time intervals ranging from 0 to 50 min were performed (Figure 5). From the thermocycler amplification data (Figure 5A), we know that 10^4 copies/μL of virus amplify in 17 min, while 10 copies/μL of virus amplify in 25 ± 1.4 min. For electrical testing of VTM samples spiked with 104 copies/μL of inactivated virus, 6 amplification cycles in the range of interest were analyzed (Figure 5B). No significant difference in the Dirac point shift was obtained for amplification time ≤10 min. However, a statistically significant variation in the Dirac point was found for amplification time ≥15 min. This demonstrates that no more than 15 min of amplification is required for highly concentrated samples. Similarly, for electrical testing of VTM samples spiked with 10 copies/μL of inactivated virus, 7 amplification times in the range of interest were analyzed (Figure 5C). In this case, while no significant difference in the Dirac point shift was obtained from amplification time ≤25 min, a statistically significant variation was found for amplification time ≥30 min. This demonstrates that no more than 30 min of amplification is required for the low concentrated samples. Therefore, we can conclude that 30 min is the amplification time required to distinguish positive samples (≥10 copies/μL) from negative samples. In addition, we found in the control measurements that the Dirac point shifts at the end of various reaction times were inversely proportional to the starting concentration of the RNA in the sample. This suggests that quantitative end-point measurements could be possible, but a more detailed characterization is needed before such a claim can be made.

Detection of the SARS-CoV-2 virus in VTM clinical samples. The performance of the developed crumpled graphene FET biosensors was also assessed by the analysis of VTM clinical samples (Figure 6). The device was validated using 20 clinical samples (10 known positives and 10 known negatives) obtained from OSF Healthcare, Peoria, IL, through an approved institutional review board (OSF Peoria IRB # 1602513 via the University of Illinois College of Medicine with a waiver for consent). Samples were collected following clinical gold standard techniques (using an NP swab) and then frozen. We received VTM discards prior to the RNA purification step and the results of the RT-PCR tests performed by OSF Healthcare.

Comparable to the results obtained with the spiked samples, the negative samples produced a large shift in the Dirac point, while the positive samples produced a smaller distinguishable variation (Figure 6A). First, 10 known positive and 10 known negative clinical samples were amplified following the procedure described previously (RT-LAMP; 65 °C, 50 min). Then, the amplified products were incubated (20 min) in the cgFET device and the variation in the Dirac point was calculated. As can be seen in Figure 6B,C, the negative samples produced a large shift in the range from 68 to 118 mV. On the other hand, the shift obtained with the positive samples was <29 mV in all cases. With this data, the decision threshold was determined to be 48.66 mV by receiver operating characteristic (ROC) curve analysis. Using this decision threshold, three positive samples were retested, but only after 30 min of amplification time. These three samples were chosen as they are the ones with the latest amplification time in the RT-LAMP analysis (lowest viral load). As illustrated in Figure 6D, the variation in the Dirac point was again below the decision threshold. Therefore, 30 min of isothermal amplification was shown to be sufficient to correctly distinguish positive from negative clinical samples. The raw data ($I-V$ curves) of variation in the Dirac point of these samples is given in the Supporting Information (Figure S3). The RT-LAMP amplification curves and a table showing the RT-PCR C_t values (control) is shown in the Supporting Information (Figure S4 and Table S2). The ROC curve analysis performed with the results of Figure 6B can be seen in Figure 6E. Likewise, the summary of the biosensor performance (sensitivity and specificity = 100%) is shown in Figure 6F.

It is important to mention that in this paper we confirmed RT-LAMP amplification using a thermocycler, only for characterization purposes. However, to successfully amplify samples prior to electrical analysis, the only instrumentation required is a simple heating block that can be set to 65 °C.

Although other graphene-based devices used for the detection of SARS-CoV-2 from clinical samples can be found in the literature,[11,20,24] none of these have implemented the crumpled graphene approach. The use of the crumpled graphene approach gives our device the ability to offer a better decision threshold (100% accuracy, sensitivity and specificity). Furthermore, although our detection protocol requires isothermal amplification, unlike the devices proposed in the literature, our cgFET biosensor does not require kits or protocols for RNA purification, gold nanoparticles, hybridization, or functionalization of molecules on the surface of graphene, which considerably reduces the cost.

CONCLUSIONS

We have developed an electrical point-of-care device for the detection of SARS-CoV-2 virus amplification. This crumpled graphene-based FET biosensor was able to distinguish VTM positive clinical samples from VTM negative clinical samples with 100% sensitivity, and specificity. Our platform can also decrease the detection time to ∼60 min (amplification ∼30 min and cgFET measurement ∼30 min). The detection

https://doi.org/10.1021/acssensors.1c01937
ACS Sens. XXXX, XXX, XXX−XXX

principle, which is based on isothermal RT-LAMP amplification, primer consumption, and noncovalent $\pi-\pi$ stacking interactions, facilitates the development of cost-effective devices that require minimal instrumentation. Future innovations in this technology will focus on the miniaturization of cgFET devices and on the development of CMOS-compatible mass fabrication processes. Although the device developed in this article was applied and validated for the SARS-CoV-2 virus, this biosensor could easily be adapted to the detection of other pathogens when the corresponding RT-LAMP primers are available.

■ ASSOCIATED CONTENT

Supporting Information

The Supporting Information is available free of charge at https://pubs.acs.org/doi/10.1021/acssensors.1c01937.

Experimental details of the materials and methods, RT-LAMP primer sequences (Table S1), Raman spectra of adenine absorbed on crumpled graphene (Figure S1), 2D images and cross-section profiles of the AFM height and phase of flat and crumpled graphene surfaces (Figure S2), $I-V$ curves of crumpled graphene FET sensors of 3 known positive clinical samples with shortened amplification time (RT-LAMP; 65 °C, 30 min) on cgFET (Figure S3), detection of the SARS-CoV-2 virus in 25% VTM clinical samples using the off-chip RT-LAMP assay performed with the EvaGreen dye (Figure S4), summary of the RT-PCR Ct values of the VTM clinical samples tested; RT-PCR tests performed by OSF Healthcare (Table S2), end-point measurement of the Dirac point shift of primers adsorption on cgFET with different concentrations (Figure S5), fabrication of crumpled graphene on the polystyrene substrate (Figure S6), geometry and dimension of chamber and gate electrode of detection cell for virus testing (Figure S7), charge transfer characteristics of the flat and crumpled graphene FET devices (Figure S8) (PDF)

■ AUTHOR INFORMATION

Corresponding Authors

Enrique Valera − *Nick Holonyak Jr. Micro and Nanotechnology Laboratory, University of Illinois at Urbana-Champaign, Urbana, Illinois 61801, United States; Department of Bioengineering, University of Illinois at Urbana-Champaign, Urbana, Illinois 61801, United States;* orcid.org/0000-0003-1359-6619; Email: evalerac@illinois.edu

Rashid Bashir − *Nick Holonyak Jr. Micro and Nanotechnology Laboratory, University of Illinois at Urbana-Champaign, Urbana, Illinois 61801, United States; Department of Bioengineering, University of Illinois at Urbana-Champaign, Urbana, Illinois 61801, United States; Department of Biomedical and Translational Science, Carle Illinois College of Medicine, Urbana, Illinois 61801, United States;* orcid.org/0000-0002-7225-9180; Email: rbashir@illinois.edu

Authors

Insu Park − *Nick Holonyak Jr. Micro and Nanotechnology Laboratory, University of Illinois at Urbana-Champaign, Urbana, Illinois 61801, United States*

Jongwon Lim − *Nick Holonyak Jr. Micro and Nanotechnology Laboratory, University of Illinois at Urbana-Champaign, Urbana, Illinois 61801, United States; Department of Bioengineering, University of Illinois at Urbana-Champaign, Urbana, Illinois 61801, United States*

Seungyong You − *Nick Holonyak Jr. Micro and Nanotechnology Laboratory, University of Illinois at Urbana-Champaign, Urbana, Illinois 61801, United States*

Michael Taeyoung Hwang − *Department of BioNano Technology, Gachon University, Seongnam 13120 Gyeonggi, Republic of Korea*

Jaehong Kwon − *Department of Chemical and Biomolecular Engineering, University of Illinois at Urbana-Champaign, Urbana, Illinois 61801, United States*

Katherine Koprowski − *Department of Agricultural and Biological Engineering, University of Illinois at Urbana-Champaign, Urbana, Illinois 61801, United States*

Sungdae Kim − *Department of Chemical and Biomolecular Engineering, University of Illinois at Urbana-Champaign, Urbana, Illinois 61801, United States*

John Heredia − *Department of Bioengineering, University of Illinois at Urbana-Champaign, Urbana, Illinois 61801, United States*

Sarah A. Stewart de Ramirez − *Department of Bioengineering, University of Illinois at Urbana-Champaign, Urbana, Illinois 61801, United States; Emergency Medicine, University of Illinois College of Medicine at Peoria & OSF Healthcare, Peoria, Illinois 61637, United States*

Complete contact information is available at: https://pubs.acs.org/10.1021/acssensors.1c01937

Author Contributions

○I.P. and J.L. contributed equally to this work. I.P., J.L., E.V., and R.B. designed the research. E.V., S.A.S.d.R., and R.B. designed the clinical sample collection protocols. I.P., J.L., S.Y., M.T.H., J.K., K.K., S.K., and J.H. performed the research. I.P., J.L., E.V., and R.B. analyzed data. E.V., I.P., J.L., K.K., and R.B. wrote the paper.

Notes

The authors declare no competing financial interest.

■ ACKNOWLEDGMENTS

The authors would like to thank the National Science Foundation for a Rapid Response Research (RAPID) grant (Award 2028431) and Jump Applied Research through Community Health through Engineering and Simulation (ARCHES) endowment through the Health Care Engineering Systems Center at UIUC to R.B. and E.V. The authors also thank the ACES Undergraduate Research Scholarship Program for providing support to this research endeavor to K.K. The authors thank Sara Riggenbach, Gabriel Koch, and Bill Bond of OSF Healthcare (Peoria, IL) for their support of the IRB # 1602513 and patient sample acquisition for this study. The following reagent was obtained through BEI Resources, NIAID, NIH: SARS-Related Coronavirus 2, Isolate USA-WA1/2020, γ-Irradiated, NR-52287, contributed by the Centers for Disease Control and Prevention.

■ REFERENCES

(1) Valera, E.; Jankelow, A.; Lim, J.; Kindratenko, V.; Ganguli, A.; White, K.; Kumar, J.; Bashir, R. COVID-19 Point-of-Care Diagnostics: Present and Future. *ACS Nano* **2021**, *15*, 7899−7906.

(2) Mayo-Clinic COVID-19 Diagnostic Testing. https://www.mayoclinic.org/tests-procedures/covid-19-diagnostic-test/about/pac-20488900 (accessed August 16, 2021).
(3) Ganguli, A.; Mostafa, A.; Berger, J.; Aydin, M. Y.; Sun, F.; Ramirez, S. A. S.; Valera, E.; Cunningham, B. T.; King, W. P.; Bashir, R. Rapid isothermal amplification and portable detection system for SARS-CoV-2. *Proc. Natl. Acad. Sci. U.S.A.* **2020**, *117*, 22727−22735.
(4) Zhu, H.; Zhang, H.; Ni, S.; Korabecná, M.; Yobas, L.; Neuzil, P. The vision of point-of-care PCR tests for the COVID-19 pandemic and beyond. *TrAC, Trends Anal. Chem.* **2020**, *130*, No. 115984.
(5) Centers for Disease Control and Prevention. COVID-19 Vaccinations in the United States. https://covid.cdc.gov/covid-data-tracker/#vaccinations_vacc-total-admin-rate-total (accessed August 16, 2021).
(6) Bleier, B. S.; Murugappan, R., Jr.; Lane, A. P. COVID-19 Vaccines May Not Prevent Nasal SARS-CoV-2 Infection and Asymptomatic Transmission. *Otolaryngol. Head Neck Surg.* **2021**, *164*, 305−307.
(7) Centers for Disease Control and Prevention. Frequently Asked Questions about COVID-19 Vaccination. https://www.cdc.gov/coronavirus/2019-ncov/vaccines/faq.html (accessed August 16, 2021).
(8) de Puig, H.; Lee, R. A.; Najjar, D.; Tan, X.; Soekensen, L. R.; Angenent-Mari, N. M.; Donghia, N. M.; Weckman, N. E.; Ory, A.; Ng, C. F.; Nguyen, P. Q.; Mao, A. S.; Ferrante, T. C.; Lansberry, G.; Sallum, H.; Niemi, J.; Collins, J. J. Minimally instrumented SHERLOCK (miSHERLOCK) for CRISPR-based point-of-care diagnosis of SARS-CoV-2 and emerging variants. *Sci. Adv.* **2021**, *7*, No. eabh2944.
(9) Wang, D.; He, S.; Wang, X.; Yan, Y.; Liu, J.; Wu, S.; Liu, S.; Lei, Y.; Chen, M.; Li, L.; Zhang, J.; Zhang, L.; Hu, X.; Zheng, X.; Bai, J.; Zhang, Y.; Zhang, Y.; Song, M.; Tang, Y. Rapid lateral flow immunoassay for the fluorescence detection of SARS-CoV-2 RNA. *Nat. Biomed. Eng.* **2020**, *4*, 1150−1158.
(10) Diaz, L. M.; Johnson, B. E.; Jenkins, D. M. Real-time optical analysis of a colorimetric LAMP assay for SARS-CoV-2 in saliva with a handheld instrument improves accuracy compared to endpoint assessment, 2021. DOI: 10.1101/2021.01.13.21249412.
(11) Seo, G.; Lee, G.; Kim, M. J.; Baek, S.-H.; Choi, M.; Ku, K. B.; Lee, C.-S.; Jun, S.; Park, D.; Kim, H. G.; Kim, S.-J.; Lee, J.-O.; Kim, B. T.; Park, E. C.; Kim, S. I. Rapid Detection of COVID-19 Causative Virus (SARS-CoV-2) in Human Nasopharyngeal Swab Specimens Using Field-Effect Transistor-Based Biosensor. *ACS Nano* **2020**, *14*, 5135−5142.
(12) Hwang, M. T.; Heiranian, M.; Kim, Y.; You, S.; Leem, J.; Taqieddin, A.; Faramarzi, V.; Jing, Y.; Park, I.; van de Zande, A. M.; Nam, S.; Aluru, N. R.; Bashir, R. Ultrasensitive detection of nucleic acids using deformed graphene channel field effect biosensors. *Nat. Commun.* **2020**, *11*, No. 1543.
(13) Ping, J.; Vishnubhotla, R.; Vrudhula, A.; Johnson, A. T. C. Scalable Production of High-Sensitivity, Label-Free DNA Biosensors Based on Back-Gated Graphene Field Effect Transistors. *ACS Nano* **2016**, *10*, 8700−8704.
(14) Hajian, R.; Balderston, S.; Tran, T.; deBoer, T.; Etienne, J.; Sandhu, M.; Wauford, N. A.; Chung, J.-Y.; Nokes, J.; Athaiya, M.; Paredes, J.; Peytavi, R.; Goldsmith, B.; Murthy, N.; Conboy, I. M.; Aran, K. Detection of unamplified target genes via CRISPR−Cas9 immobilized on a graphene field-effect transistor. *Nat. Biomed. Eng.* **2019**, *3*, 427−437.
(15) Hwang, M. T.; Landon, P. B.; Lee, J.; Choi, D.; Mo, A. H.; Glinsky, G.; Lal, R. Highly specific SNP detection using 2D graphene electronics and DNA strand displacement. *Proc. Natl. Acad. Sci. U.S.A.* **2016**, *113*, 7088−7093.
(16) Ganguli, A.; Faramarzi, V.; Mostafa, A.; Hwang, M. T.; You, S.; Bashir, R. High Sensitivity Graphene Field Effect Transistor-Based Detection of DNA Amplification. *Adv. Funct. Mater.* **2020**, *30*, No. 2001031.
(17) Kang, P.; Wang, M. C.; Knapp, P. M.; Nam, S. Crumpled Graphene Photodetector with Enhanced, Strain-Tunable, and Wavelength-Selective Photoresponsivity. *Adv. Mater.* **2016**, *28*, 4639−4645.
(18) Ganguli, A.; Mostafa, A.; Berger, J.; Lim, J.; Araud, E.; Baek, J.; Ramirez, S. A. S.; Baltaji, A.; Roth, K.; Aamir, M.; Aedma, S.; Mady, M.; Mahajan, P.; Sathe, S.; Johnson, M.; White, K.; Kumar, J.; Valera, E.; Bashir, R. Reverse Transcription Loop-Mediated Isothermal Amplification Assay for Ultrasensitive Detection of SARS-CoV-2 in Saliva and Viral Transport Medium Clinical Samples. *Anal. Chem.* **2021**, *93*, 7797−7807.
(19) Hwang, M. T.; Park, I.; Heiranian, M.; Taqieddin, A.; You, S.; Faramarzi, V.; Pak, A. A.; Zande, A. M. vd.; Aluru, N. R.; Bashir, R. Ultrasensitive Detection of Dopamine, IL-6 and SARSCoV-2 Proteins on Crumpled Graphene FET Biosensor. *Adv. Mater. Technol.* **2021**, *6*, No. 2100712.
(20) Li, J.; Wu, D.; Yu, Y.; Li, T.; Li, K.; Xiao, M.-M.; Li, Y.; Zhang, Z.-Y.; Zhang, G.-J. Rapid and unamplified identification of COVID-19 with morpholino-modified graphene field-effect transistor nanosensor. *Biosens. Bioelectron.* **2021**, *183*, No. 113206.
(21) Mensah, K.; Cissé, I.; Pierret, A.; Rosticher, M.; Palomo, J.; Morfin, P.; Plaçais, B.; Bockelmann, U. DNA Hybridization Measured with Graphene Transistor Arrays. *Adv. Healthcare Mater.* **2020**, *9*, No. 2000260.
(22) D'Amico, F.; Cammisuli, F.; Addobbati, R.; Rizzardi, C.; Gessini, A.; Masciovecchio, C.; Rossi, B.; Pascolo, L. Oxidative damage in DNA bases revealed by UV resonant Raman spectroscopy. *Analyst* **2015**, *140*, 1477−1485.
(23) Stark, M.; Möller, C.; Müller, D. J.; Guckenberger, R. From Images to Interactions: High-Resolution Phase Imaging in Tapping-Mode Atomic Force Microscopy. *Biophys. J.* **2001**, *80*, 3009−3018.
(24) Alafeef, M.; Dighe, K.; Moitra, P.; Pan, D. Rapid, Ultrasensitive, and Quantitative Detection of SARS-CoV-2 Using Antisense Oligonucleotides Directed Electrochemical Biosensor Chip. *ACS Nano* **2020**, *14*, 17028−17045.

https://doi.org/10.1021/acssensors.1c01937
ACS Sens. XXXX, XXX, XXX−XXX